



Dual green hemostatic sponges constructed by collagen fibers disintegrated from *Halocynthia roretzi* by a shortcut method

Cuicui Ding^a, Kuan Cheng^a, Yue Wang^a, Yifan Yi^a, Xiaohong Chen^b, Jingyi Li^{c,*}, Kaiwen Liang^d, Min Zhang^{d,**}

^a College of Ecological Environment and Urban Construction, Fujian University of Technology, Fuzhou, 350118, PR China

^b Department of Ophthalmology, The 900th Hospital of Joint Logistic Support Force, PLA (Clinical Medical College of Fujian Medical University, Dongfang Hospital Affiliated to Xiamen University), Fuzhou, 350025, PR China

^c Department of Biochemistry and Molecular Biology, School of Basic Medical Sciences, Fujian Medical University, Fuzhou, 350122, PR China

^d College of Material Engineering, Fujian Agriculture and Forestry University, Fuzhou, 350108, PR China

ARTICLE INFO

Keywords:

Collagen fiber
Halocynthia roretzi
Hemostatic sponge

ABSTRACT

Recently, biomacromolecules have received considerable attention in hemostatic materials. Collagen, an ideal candidate for hemostatic sponges due to its involvement in the clotting process, has been facing challenges in extraction from raw materials, which is time-consuming, expensive, and limited by cultural and religious restrictions associated with traditional livestock and poultry sources. To address these issues, this study explored a new shortcut method that using wild *Halocynthia roretzi* (HR), a marine fouling organism, as a raw material for developing HR collagen fiber sponge (HRCFs), which employed urea to disrupt hydrogen bonds between collagen fiber aggregates. This method simplifies traditional complex manufacturing processes while utilized marine waste, thus achieving dual green in terms of raw materials and manufacturing processes. FTIR results confirmed that the natural triple-helical structure of collagen was preserved. HRCFs exhibit a blood absorption ratio of 2000–3500 %, attributed to their microporous structure, as demonstrated by kinetic studies following a capillary model. Remarkably, the cytotoxicity and hemolysis ratio of HRCFs are negligible. Furthermore, during *in vivo* hemostasis tests using rabbit ear and kidney models, HRCFs significantly reduce blood loss and shorten hemostasis time compared to commercial gelatin sponge and gauze, benefiting from the capillary effect and collagen's coagulation activity. This study provides new insights into the design of collagen-based hemostatic biomaterials, especially in terms of both raw material and green manufacturing processes.

1. Introduction

Uncontrolled bleeding, including severe visceral bleeding, is a leading cause of death in emergency situations such as warfare, traffic accidents, and clinical surgeries [1]. Although gauze is commonly used for hemostasis in first aid, its effectiveness is limited, particularly in cases of internal organ injury [2]. External intervention may be necessary to physically hemostasis, but this can increase the risk of additional injury to the patient. Therefore, there is a pressing need for more effective hemostatic materials that can quickly and safely control severe bleeding. Sponges, with their highly porous, three-dimensional structure, offer a promising solution for effectively absorbing and controlling bleeding in emergency situations. By providing ample space for blood

cells to attach, sponges can help to reduce the risk of additional injury to the patient during external intervention [3].

Recently, synthetic polymers, such as poly (ethylene glycol) [4] and poly (vinyl alcohol) [5], have gained extensive research in the development of hemostatic sponges. However, these materials exhibit limited biocompatibility and insufficient biological activity [6]. Therefore, biomacromolecules like collagen [7], chitosan [8] and cellulose [9] have emerged as a promising alternative due to their wide availability, cost-effectiveness, biocompatibility, and biodegradability [10]. Collagen, as the most abundant structural protein in mammals, constitutes the principal component of the extracellular matrix. A great deal of research has demonstrated that collagen plays a role in endogenous coagulation and facilitates blood clotting [11–15]. Briefly, when a blood

* Corresponding author.

** Corresponding author.

E-mail addresses: lijingyi@fjmu.edu.cn (J. Li), mzhang@fafu.edu.cn (M. Zhang).

<https://doi.org/10.1016/j.mtbio.2024.100946>

Received 27 October 2023; Received in revised form 27 December 2023; Accepted 3 January 2024

Available online 7 January 2024

2590-0064/© 2024 Published by Elsevier Ltd. This is an open access article under the CC BY-NC-ND license (<http://creativecommons.org/licenses/by-nc-nd/4.0/>).

vessel ruptures, blood encounters negatively charged collagen beneath the skin, triggering a cascade of coagulation factors that activate the prothrombin complex, ultimately leading to the clot formation. In recent years, researchers have developed various collagen-based materials [16–18]. However, these kind of materials have two disadvantages: I) most of them are derived from terrestrial livestock and poultry such as cattle and swine [16], which are limited to cultural and religious constraints [18], as well as the risk of zoonotic diseases such as foot-and-mouth disease and avian influenza [16], II) the extraction of collagen is mostly carried out using acid-enzyme method, which suffer from deficiencies such as the requirement for multiple reagents, long cycles, and high costs [17].

Regarding the first deficiency, there is growing interest in alternative collagen sources, such as marine organisms or fish by-products [19–21]. For instance, Govindharaj et al. [19] successfully isolated collagen from discarded marine Eel skin and utilized 3D printing technology to fabricate tissue engineering scaffolds. Recently, the research and development of low-value marine fouling organism have aroused researchers' concern. Wild *Halocynthia roretzi* (HR), a marine benthic organism, is composed of tunic and inner tissue, with the inner tissue rich in collagen [22]. These filter-feeding hermaphroditic organisms possess remarkable reproductive capabilities and a broad range of environmental adaptability [23]. Wild HR tend to attach themselves to solid surfaces such as ships and fishing nets, as well as compete with shellfish and algae for food resources [24]. This behaviour can significantly jeopardize economic development and ecological balance, leading to their classification as fouling organisms or invasive species [25,26]. Currently, research on HR primarily focuses on the extraction of nanocellulose from the tunic of HR to produce medical materials [27–29]. Additionally, other studies concentrate on extracting terpenoids [30] and astaxanthin [31] from the inner tissues of HR. As far as we know, the utilization of collagen in HR has rarely been reported. The rational development and utilization of HR not only circumvents the limitations of collagen derived from terrestrial livestock and poultry sources, but also effectively addresses waste in the marine environment, turning waste into valuable resources.

Regarding the second deficiency, current research endeavours primarily revolve around refining the efficiency of conventional collagen extraction methods [32], including the integration of ultrasound technology within the extraction process. Nonetheless, these technological advancements still face the challenges of complex extraction procedure and the requirements of multiple reagents. Considering that hydrogen bonds are the primary connections between collagen fibers [33], one possible approach for extracting micrometre-sized collagen fibers is to directly disrupt the hydrogen bonds between the fibers. As early as 2004, Zhang et al. [34] successfully dissolved cellulose at low temperatures using a NaOH/urea aqueous solution, pioneering the technique of polymer low temperature dissolution. In this process, NaOH acts as an alkaline catalyst, facilitating the hydrolysis reaction of cellulose, while urea serves as a hydrogen bond disruptor, enhancing the solubility of cellulose. Inspired by the above work, our previous study has demonstrated that urea can disrupt the hydrogen bonds between collagen aggregates, leading to a fiber dissociation effect and thereby increasing the solubility of collagen in acidic environments [35]. Pei et al. [36] employed a NaOH/urea aqueous solution, along with freeze-thaw cycles and ultrasonic treatment, to extract collagen fibers from bovine tendons. These previous studies have indeed paved the way for novel approaches to collagen extraction. Nevertheless, the reliance on environmentally unfriendly solvents, such as acids and alkalis, persists. To achieve greener production, we have developed an innovative method for collagen extraction, where the synergistic effect of high-speed homogenization and urea-induced disruption of hydrogen bonds effectively disintegrated the collagen fibers within the inner tissue of HR. Subsequently, these micrometre-sized fibers were dispersed in deionized water and then subjected to lyophilization, resulting in the formation of HR collagen fiber sponge (HRCFs). This novel preparation method of

Table 1

Sample names under different treatment conditions.

Sample name	Collagen content (mg/mL)	Urea concentration (mg/mL)
HR15(u1)	15	1
HR20(u1)	20	1
HR25(u1)	25	1
HR30(u1)	30	1
HR50(u1)	50	1
HR15(u3)	15	3
HR20(u3)	20	3
HR25(u3)	25	3
HR30(u3)	30	3
HR50(u3)	50	3
HR15(u5)	15	5
HR20(u5)	20	5
HR25(u5)	25	5
HR30(u5)	30	5
HR50(u5)	50	5

collagen sponge completely circumvents the use of acid and alkali solvents, with the only solvents involved are urea and NaCl, which can be recycled and reused. Moreover, this process significantly shortens the cycle for collagen and simplifies the preparation steps compared to previous methods, thus realizing a dual green from raw materials to the preparation process.

In this study, a novel collagen fiber sponge as hemostatic material was obtained using a shortcut method with HR as the raw material. The structure, mechanical properties, liquid absorption capacity, and blood clotting ability of HRCFs were characterized. Furthermore, the hemostatic properties of HRCFs were comprehensively investigated using animal experimental models. The HRCFs developed in this study not only provides ideas for the development of marine organisms, but also provides theoretical guidance and practical significance for the development of green hemostatic materials.

2. Materials and methods

2.1. Materials

Wild HRs were caught alive in shallow sea of Fujian, China. Urea, sodium chloride and calcium chloride are of analytical grade and purchased from Aladdin Co., Ltd. (China). Gelatin hemostatic sponge (Gelatin) was purchased from Nanchang Hushida Medical Technology Co., Ltd. (China). Medical gauze (Gauze) was purchased from Jiangxi Zhizheng Medical Instrument Co., Ltd (China). Anticoagulated rabbit whole blood was purchased from Beijing Penglichi Science and Technology Co., Ltd (China). Deionized (DI) water was used for all aqueous samples.

2.2. Preparation of HRCFs

The inner tissues were obtained after removing the HR's tunic. The body wall muscle tissue was obtained from the inner tissues after removing the stomach, intestines, and reproductive glands. The muscle tissue was thoroughly rinsed with DI water and chopped and then soaked in a NaCl solution (2 mol/L) at a ratio of 1:15 (v/v) for 12 h at 4 °C to remove impurity proteins, and then rinsed 3 times with DI water. The filtered resultants were dispersed into different concentrations of urea solution (1 mg/mL, 3 mg/mL, 5 mg/mL) at a ratio of 1:10 (v/v) and stirred at 4 °C for 3 min using a homogenizer (10,000 rpm), and then frozen in a refrigerator for 6 h. The frozen mixture was thawed at 4 °C for 10 min and then stirred for 3 min using the homogenizer (10,000 rpm). The HR collagen fibers were collected from the above mixture by filtration and rinsed 3 times with DI water. After the resultants were dehydrated by freeze-drying, different weights of collagen fibers were homogenized in the same volume of DI water. Finally, a series of HRCFs were obtained through freeze-drying and their names are shown in

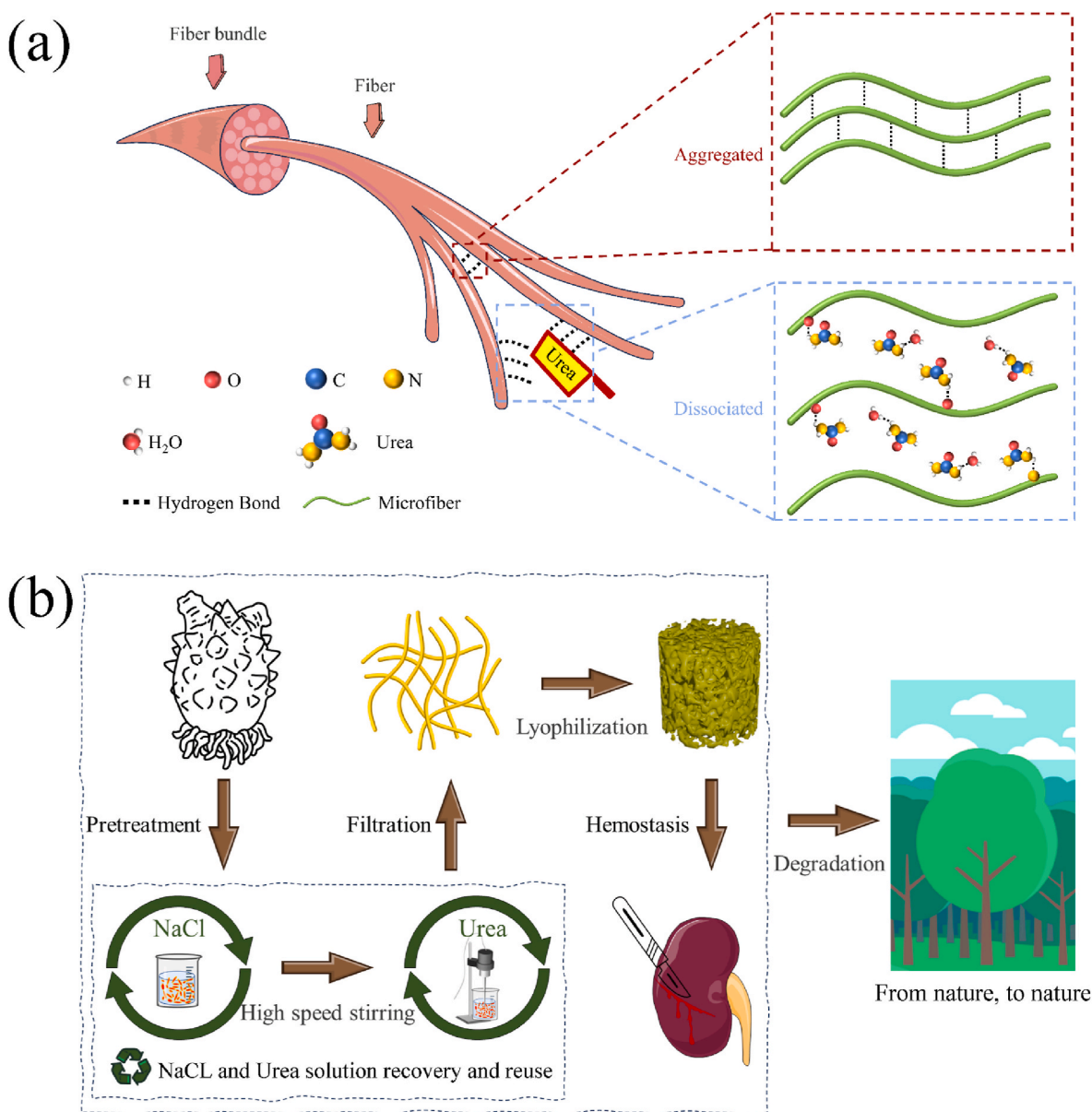


Fig. 1. (a) Dissociation rationale of fibers. (b) Fabrication process of HRCFs.

Table 1. During the above process, sodium chloride solution and urea solution were recovered and reused.

2.3. Biodegradation experiment

The biodegradation experiment was conducted according to the reported method [37]. Briefly, preweighted HRCFs was buried 5 cm below the soil surface, and its weight loss over time was recorded. During this experiment, the mean temperature and relative humidity of the soil was about 25.0 °C and 21.0 %, respectively. The weight loss of HRCFs was calculated according to the formula (eqn (1)):

$$\text{Weight loss (\%)} = \frac{W_a - W_b}{W_a} \times 100\% \quad (1)$$

where W_a and W_b denote the weight of the HRCFs before and after being buried in the soil, respectively.

2.4. Characterization

Fourier-transform infrared (FTIR) spectra of HRCFs was tested in a FTIR spectrometer (NICOLET IS 50, USA) by the potassium bromide tablet method. Each spectrum was the average of 32 scans between 4000 and 400 cm^{-1} at a resolution of 4 cm^{-1} . The microstructure of HRCFs was observed by field emission scanning electron microscopy (FESEM; Thermo Verios G4, USA) at an accelerating voltage of 3 kV.

2.5. Mechanical property

The compression performance of HRCFs was measured by an electronic universal testing machine (Lishi LD22-102, China). The cylindrical HRCFs (15 mm in diameter and height) was compressed to 70 % of its original height, and the corresponding stress-strain curves were plotted.

2.6. Porosity

The porosity measurements of HRCFs were conducted using the

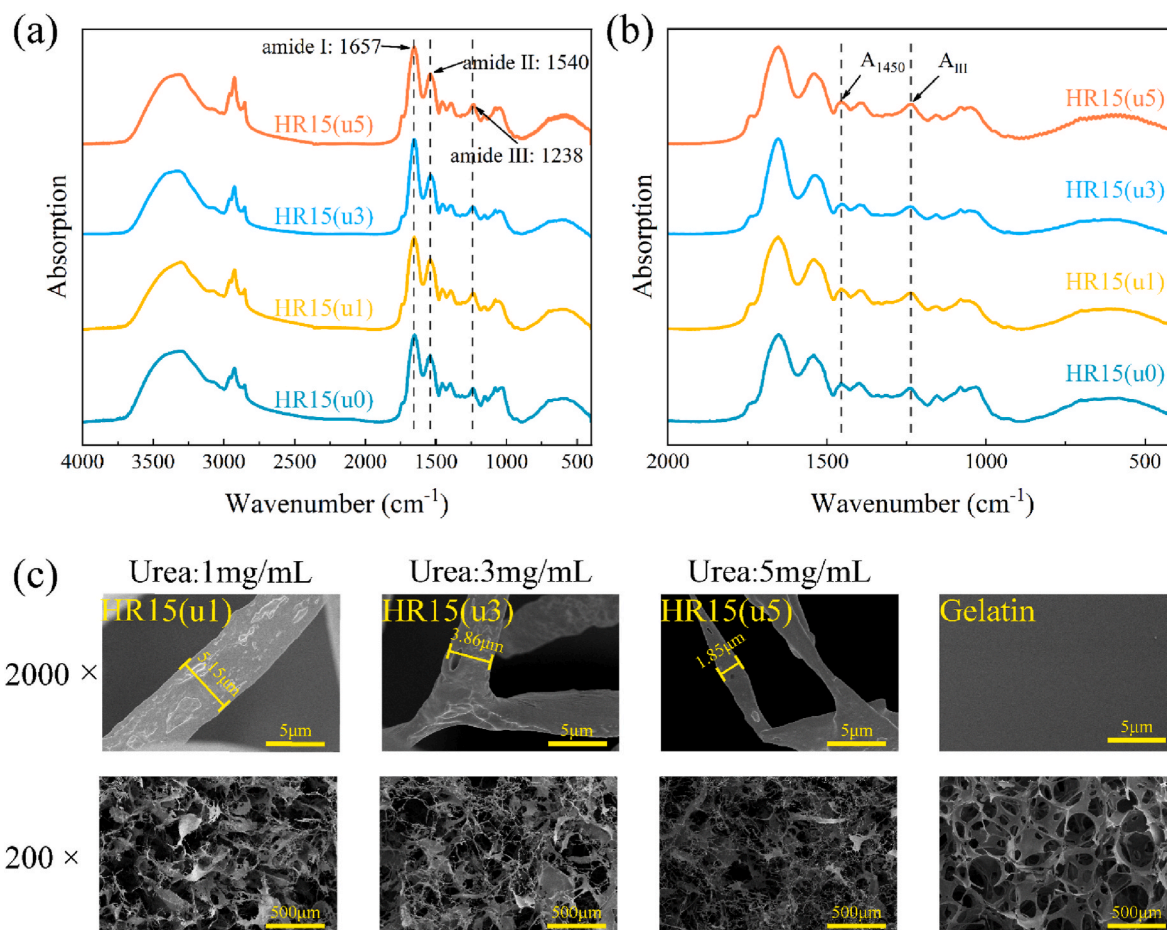


Fig. 2. FTIR spectra of HR15(u0), HR15(u1), HR15(u3), and HR15(u5) at wavenumbers from (a) 4000–400 cm^{-1} , (b) 2000–400 cm^{-1} , (c) FESEM images of HR15 (u1), HR15(u3), HR15(u5), and Gelatin at different magnifications.

liquid displacement method, as previously described [38]. Briefly, pre-weighted HRCFs were fully saturated by immersion in ethanol, and the weight of the saturated HRCFs was recorded. The porosity was then calculated according to the formula (eqn (2)):

$$\text{Porosity (\%)} = \frac{W_1 - W_0}{\rho V} \times 100\% \quad (2)$$

where W_0 and W_1 denote the weight of the HRCFs before and after immersion in ethanol, respectively. The ρ represents the density of ethanol (0.789 g/cm^3), and V is the volume of HRCFs.

2.7. Liquid absorption ratio

The Liquid absorption ratio of HRCFs was determined according to the reported method [39]. Briefly, preweighted HRCFs was submerged in either water or blood for 10 min, after which the weight of the absorbed HRCFs was recorded. The water or blood absorption ratio of HRCFs was calculated according to the formula (eqn (3)):

$$\text{Water or blood absorption ratio (\%)} = \frac{M_1 - M_0}{M_0} \times 100\% \quad (3)$$

where M_0 and M_1 denote the weight of the HRCFs before and after immersion in water or blood, respectively.

2.8. Wetting performance

DI water was selected to measure the wetting performances of HRCFs. The HRCFs was cut with a size of 10 mm*10 mm*5 mm

(length*width*height). A 5 μL of DI water was dropped onto the samples surface by a 30G needle. The contact angle images were recorded by using a contact angle device (KINO SL250, USA) with different time points, and the results were analysed by CAST 3.0. The HRCFs was placed in a petri dish filled with DI water and anticoagulated rabbit whole blood, and the process of the sample absorbing the liquid through capillary action was recorded with a video camera, and the time and liquid-level in the HRCFs were recorded.

2.9. Hemostasis in vitro

The blood clotting stability [40], blood clotting index (BCI) [41] and blood cell adhesion [42] of HRCFs were evaluated referring to the previous reports. The details are available in the ESI Methods section.

2.10. Biocompatibility

According to the previous reports, the biocompatibility of HRCFs was evaluated by CCK-8 assay [7], live/dead staining assay [7] and hemolysis assay [44]. The details are available in the ESI Methods section.

2.11. Hemostasis in vivo

According to previous reports, the hemostatic effect of HRCFs was evaluated in rabbit ear puncture bleeding model [45], rabbit ear scratch bleeding model [46] and rabbit kidney scratch bleeding model [47]. The details are available in the ESI Methods section. The experimental subjects were male New Zealand white rabbits (12–13 weeks of age,

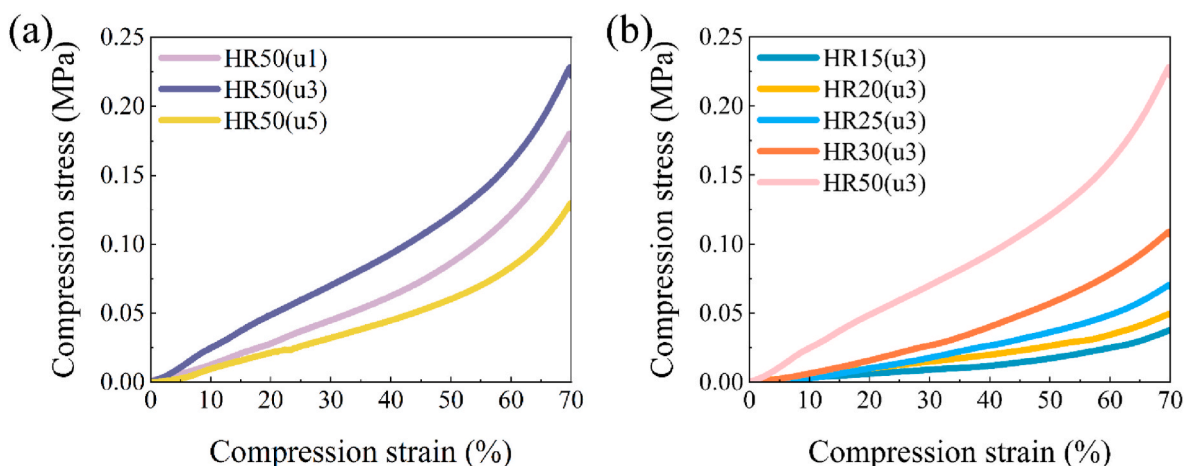


Fig. 3. (a) Compressive stress-compressive strain curves of HR50(u1), HR50(u3) and HR50(u5). (b) Compressive stress-compressive strain curves of HR15(u3)-HR50(u3).

2.3–2.5 kg of weight). This study was performed in strict accordance with the National Institutes of Health guidelines for the care and use of laboratory animals (NIH Publication No. 85-23 Rev, 1985) and was approved by the Animal Experiment Ethics Committee of Fujian Medical University, Fujian, China (IACUC FJMU 2023-0266).

2.12. Statistical analysis

Data were analysed by a one-way ANOVA using Origin 2023 software. Error bars indicate the mean \pm standard deviation (SD) of the measured values ($p < 0.05$) and the significance of difference was set as $p < 0.05$.

3. Results and discussion

3.1. Design rationale and green metrics of HRCFs

Traditional methods of collagen extraction predominantly rely on the acid-enzyme method, in which pre-treated collagen fibers within connective tissue are broken down into collagen molecules by acid and enzyme treatment. The collagen molecules reassemble to construct a collagen fiber sponge *via* freeze-drying. The process can be described by the pentadic transformation pathway of "tissue-fiber-molecule-fiber-sponge." However, this conventional process is characterized by its complexity, lengthy duration, and the use of numerous chemical reagents. To address these limitations, we propose a novel approach for the fabrication of collagen sponges using HR, a marine fouling organism, as raw materials. Our method involves the synergistic use of urea and mechanical stripping to disrupt the hydrogen bonding between collagen fibers within connective tissues. This disruption leads to the dissociation of collagen fibers into micro, enabling the production of HRCFs through the freeze-drying technique (Fig. 1(a)). The specific preparation process is depicted in Fig. 1(b), illustrating a ternary transformation pathway named as "tissue-microfiber-sponge" to produce collagen sponges (Movie S1). This innovative approach offers notable advantages over the acid-enzyme method, including a substantial reduction in the preparation cycle time, decreased chemical usage, and the possibility of solvent recycling. Notably, this method employs solely urea and sodium chloride, and impressive recovery rates of 80.44 % for urea and 91.32 % for sodium chloride through natural evaporation and crystallization way. Moreover, the HR50(u3) sample was introduced into the soil environment. Over time, the sample underwent progressive degradation attributed to the activity of microorganisms in the soil, ultimately achieving complete degradation within 15 days (Fig. S1, S2).

3.2. Structure and characteristic

To investigate the influence caused by urea to the collagen structure, infrared absorption spectra of collagen fibers treated with varying concentrations of urea were analysed. From the FTIR results of Fig. 2(a), it could be observed that HRCFs showed amide I band at 1657 cm^{-1} (for C=O stretching vibration), amide II band at 1540 cm^{-1} (for N-H wagging vibration), and amide III band at 1238 cm^{-1} (for N-H formation vibration), which are all typical characteristic peaks of collagen [16]. Moreover, the ratio of the amide III band intensity to that at 1450 cm^{-1} (A_{III}/A_{1450}) can serve as an indicator to assess the integrity of the collagen triple-helix structure [48]. In Fig. 2(b) and Table S1, it can be seen that the A_{III}/A_{1450} ratios of all the samples remained within the range of 1.009–1.151. This result indicates that the treatment with urea does not cause disruption to the triple-helical structure of collagen.

Fig. 2(c) depicts the micro-morphology of HRCFs treated with different concentrations of urea. It is evident that as the urea concentration increases, the diameter of collagen fibers in HRCFs decreases. Moreover, the HR15(u1) sample exhibits a significant presence of collagen fiber aggregates with a lamellar structure, indicating a lower degree of collagen fiber dissociation. In contrast, the quantity of lamellar structure is reduced in HR15(u3), while the network structure of HR15(u5) primarily consists of collagen microfibers. This suggests that the degree of collagen fiber dissociation increases with higher urea concentration. The internal structure of HRCFs becomes denser with a decrease in voids, corresponding to an increase in collagen fiber content (Fig. S3). Furthermore, in Fig. 2(c), the commercial hemostatic sponge (Gelatin) is observed to be composed of numerous smooth lamellar structures, forming a honeycomb mesh structure. This configuration leads to poor pore-to-pore connectivity within the sponge.

The hemostatic sponge material possesses robust mechanical properties, making it a dependable physical support, especially for compressive hemostasis. From Fig. 3(a), HR50(u1) exhibits lower compressive stress than HR50(u3), and HR50(u5) has the lowest compressive stress. The variations in the mechanical properties of the samples could be explained by the differences in their internal network structure (Fig. 2(c)). Specifically, at a urea concentration of 1 mg/mL, the lamellar collagen fiber aggregates did not dissociate sufficiently, resulting in a loosely arranged structure. Consequently, the sponge becomes more susceptible to be compressed. In contrast, under 3 mg/mL urea treatment, medium-diameter fibers were obtained which mutually reinforced with the remaining lamellar structures, enhancing the compression performance of network structure. However, at a urea concentration of 5 mg/mL, the lamellar structure predominantly dissociates into unstable fine fibers, diminishing its compressive properties.

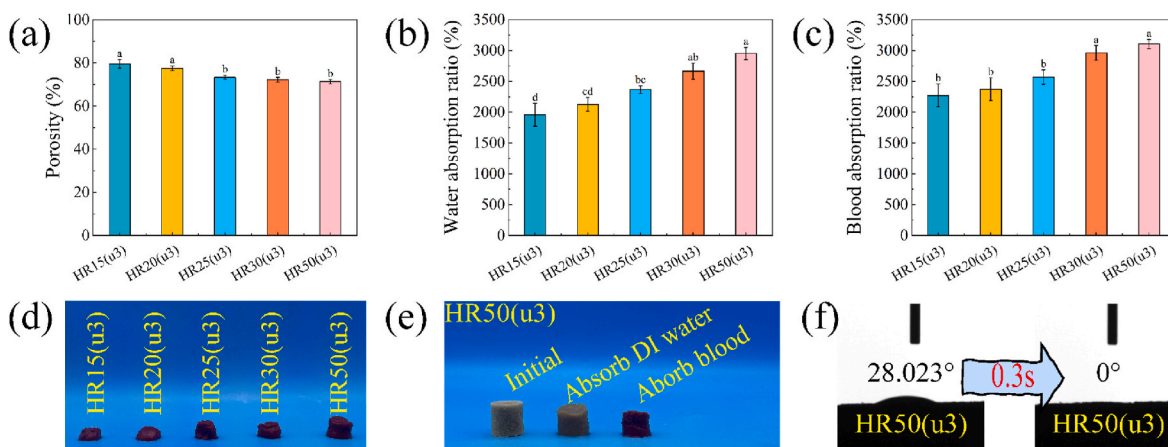


Fig. 4. (a) Porosity of HR15(u3)-HR50(u3). (b) Water absorption ratio of HR15(u3)-HR50(u3). (c) Blood absorption ratio of HR15(u3)-HR50(u3). (d) Photos of HR15(u3)-HR50(u3) after blood absorption. (e) Photos of HR50(u3) at initial, water absorption, and blood absorption. (f) Contact angle of HR50(u3) and its variation. Different letters in the bar chart indicate significant differences ($p < 0.05$) between samples.

The compressive stress of the samples increased with increasing collagen content after the same urea treatment (Fig. 3(b)). This phenomenon is also reflected in the compressive stress-compressive strain curves of HR15(u1)-HR50(u1) and HR15(u5)-HR50(u5) (Fig. S4). Since the mechanical properties of HR15(u3)-HR50(u3) are optimal, HR15(u3)-HR50(u3) was chosen as the test object in the subsequent experiments.

3.3. Physical properties

High porosity plays a crucial role in ensuring a high fluid absorption rate of the sponge and in creating a favourable environment for blood cell aggregation and adhesion. For ideal hemostatic sponges, a porosity greater than 60 % is desirable as it facilitates the efficient absorption of exudate from the wound [49]. Fig. 4(a) depicts a marginal decrease in sample porosity as the collagen fibers increases. However, it is noteworthy that the porosity of HR15(u3)-HR50(u3) remains above 70 %, indicating their significant potential for rapid liquid absorption.

The water absorption and blood absorption capacity of HR15(u3)-HR50(u3) are demonstrated in Fig. 4(b and c). These samples exhibit an impressive capability to absorb and retain liquid, with absorption capacities ranging from 20 to 30 times their own weight. Notably, the amount of liquid absorbed by the samples displays a gradient increase with the rise in collagen content. This phenomenon can be chiefly attributed to the structural stability of the sponges. HR50(u3), characterized by an interweaving network of microfibers, forms a robust three-dimensional porous structure that is self-supporting and relatively stable. Conversely, HR15(u3) with lower collagen content exhibits fewer interconnections between fibers, making its structure susceptible to collapse under the influence of liquid surface tension. Fig. 4(d) shows the photos of HR15(u3)-HR50(u3) after absorbing blood. Notably, the sample with lower collagen content becomes compressed into a ball due to liquid surface tension, whereas the higher collagen content sample demonstrates enhanced resistance against liquid surface tension, maintaining its original shape to a greater extent. Furthermore, Fig. 4(e) is the photos of HR50(u3) before and after absorption of DI water and blood.

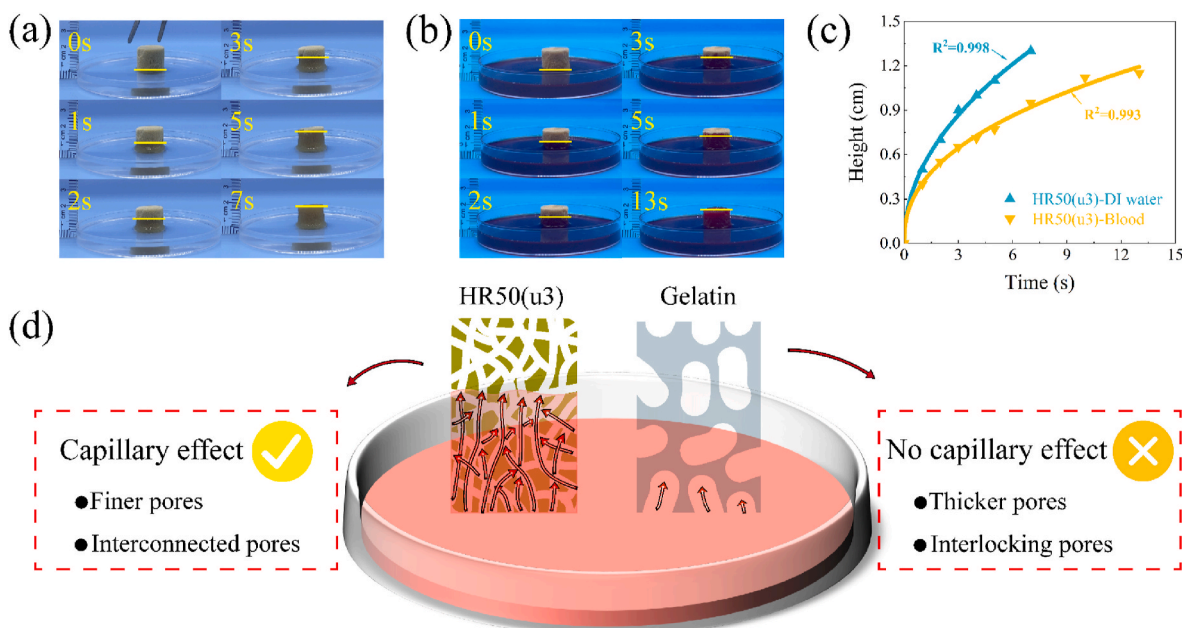


Fig. 5. The absorption height and time of HR50(u3) (a) in DI water, (b) in blood. (c) Fitted curves depicting the relationship between the height of absorbed DI water and blood over time. (d) Schematic of liquid-absorbing capacity for HR50(u3) and Gelatin.

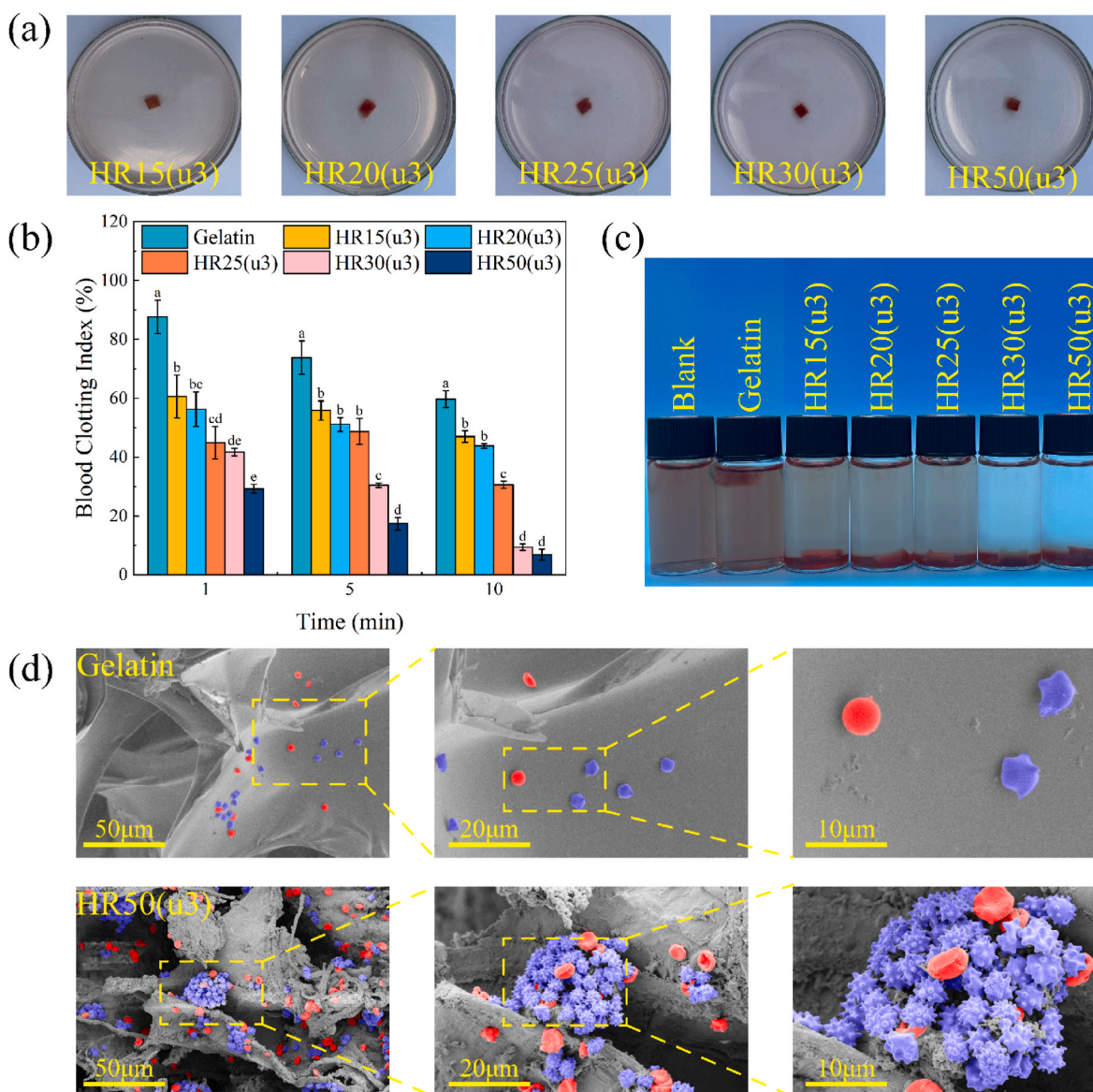


Fig. 6. Blood clotting stability of HR15(u3)-HR50(u3). (b) BCI of HR15(u3)-HR50(u3). Different letters in the bar chart indicate significant differences ($p < 0.05$) between samples. (c) Coagulation effects of HRCFs observed during BCI. (d) Interactions of HR50(u3) and Gelatin with blood cells.

Once again, the sample exhibits a remarkable ability to retain its network even after liquid absorption.

The hydrophilicity of HR50(u3) is further demonstrated in Fig. 4(f) and Movie S2. Upon contact with water, HR50(u3) exhibits remarkable hydrophilic behaviour as droplets were instantaneously absorbed within 0.3 s after contacting the sample surface, owing to its abundant pore structure and hydrophilic groups. The rapid absorption process is visually captured in Movie S2, where the initially compressed HR50(u3) is immersed in water and promptly absorbs the liquid. Notably, the sample volume swiftly expands back to its initial size.

The processes of HR50(u3) absorbing DI water and blood are shown in Fig. 5(a and b) and Movie S3. The absorption behaviour of HR50(u3) can be described by the Washburn equation [50], which states that the height of liquid absorption in the capillary is dependent on time, as shown in the following equation:

$$h^2 = \frac{r \times \gamma \times \cos \theta}{2\eta} \times t$$

where h is the height of the liquid surface, r is the average radius of the pores, γ is the surface tension of the liquid, θ is the contact angle of the

liquid in the capillary, η is the viscosity of the liquid, and t is the time. To analyse the absorption behaviour of HR50(u3) in DI water and blood, the data in Fig. 5(c) were fitted with the equation $h = at^b$. The values of a and b recorded for HR50(u3) during the absorption of DI water and blood are presented in Table S2. Notably, for DI water with lower viscosity, the value of b is approximately 0.48, which is in close agreement with the theoretical value of 0.5. For whole blood with higher viscosity, the value of b is around 0.42, which is also in proximity to the theoretical value. These findings suggest that the internal pore structure of HR50(u3) closely resembles the ideal capillary model, exhibiting low resistance to liquid flow within it (Fig. 5(d)). Furthermore, Gelatin did not exhibit capillary effect, which may be attributed to the poor connectivity between its internal pores (Fig. 2(c), Movie S3).

3.4. In vitro hemostatic properties of HRCFs

The blood clotting stability was evaluated using the mechanical oscillation method. As shown in Fig. 6(a), the samples were mechanically oscillated in saline solution, and no structural scattering was observed, indicating that the blood clots formed by the samples exhibit

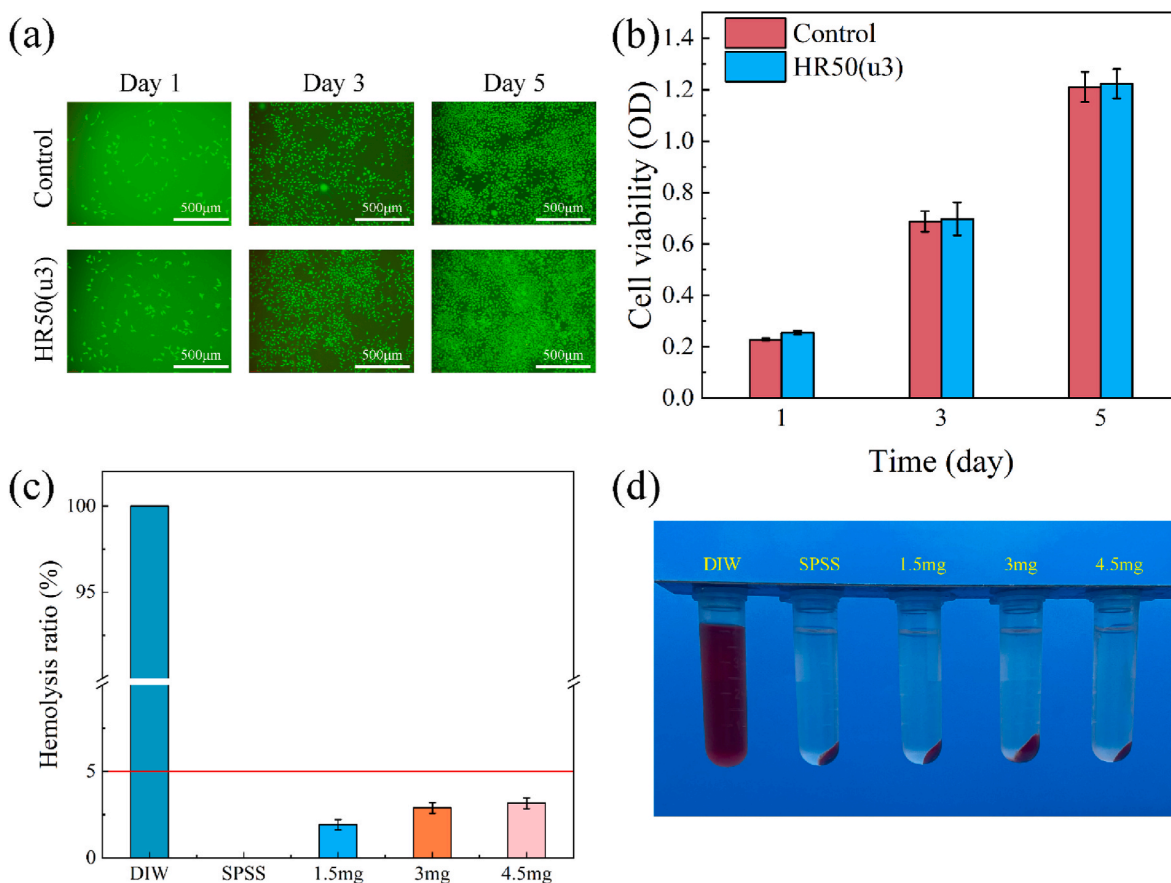


Fig. 7. (a) Cell viability study using L929 fibroblast cells via CCK-8 assay on days 1, 3, and 5 (* $p < 0.05$). (b) Representative live/dead staining images of L929 fibroblast cells on days 1, 3, and 5. (c) Hemolysis ratio of HRCFs. (d) Hemolysis effects of HRCFs observed during hemolysis test.

good structural stability. To further assess the coagulation performance, Gelatin was chosen as the control group, and the blood clot index (BCI) of the sample was measured (Fig. 6(b)). A higher BCI value indicates that fewer red blood cells entered the sample, resulting in a cloudier supernatant. Conversely, a lower BCI value indicates better coagulation performance. The BCI value of the sample gradually decreased over time (Fig. 6(b)). Additionally, under the same time conditions, the BCI value decrease gradually with an increase in the collagen content of the sample. This suggests that collagen fibers have a strong adhesive effect on platelets and can accelerate the coagulation process. In contrast, the BCI value of Gelatin is much higher than that of the sample, indicating its poor adhesion for blood cells. Fig. 6(c) depicts the coagulation effect of the materials during BCI determination. As the collagen content increased during the experiment, the colour of the DI water in the sample bottle became clearer. This indicates that more red blood cells were absorbed by the HRCFs.

To investigate the interaction between HRCFs and blood cells, HR50 (u3) was selected as the blood cell adhesion experimental subject and compared with Gelatin. As depicted in Fig. 6(d), a significant number of blood cells are observed adhering and aggregating inside HR50(u3), whereas only a few dispersed blood cells appeared on the surface of Gelatin. When platelets in the body are activated, they undergo morphological changes from a slightly convex disc shape to an irregular shape, with numerous irregular pseudopods appearing on the surface [51]. Platelets adhering to HR50(u3) display longer and more pseudopods compared to Gelatin, indicating that HR50(u3) possesses the ability to activate platelets.

3.5. Biocompatibility of HRCFs

For a hemostatic material, the evaluation of biocompatibility is essential, involving the measurement of cytotoxicity and hemolysis assays *in vitro*. The CCK-8 assay results (Fig. 7(a)) reveals a significant proliferation of L929 cells within the sample group over five days. Furthermore, Fig. 7(b) indicates that most cells in both groups remained viable, with an almost negligible presence of dead cells. Additionally, the optical density (OD) values in the sample group closely resembled those of the control group, affirming the favourable cytocompatibility of HR50(u3).

According to the requirements of ASTM F756-17 [52], the hemolysis rate of a hemostatic material should be below 5%. Fig. 7(a) shows that almost all RBCs in the positive control were lysed, resulting in the release of haemoglobin. Conversely, the negative control exhibited intact RBCs. The hemolysis rates of HRCFs with varying collagen fiber contents are significantly below 5%, with their corresponding supernatants closely resembling those of the negative control samples (Fig. 7(b)). These results indicate that HRCFs possess reliable hemocompatibility as hemostatic materials.

3.6. *In vivo* hemostatic properties of HRCFs

The *in vitro* hemostatic properties and results of hemolysis tests support the potential suitability of HRCFs as an ideal material for hemostasis. To further evaluate their hemostatic properties, animal experiments were conducted using graded bleeding volumes, including rabbit ear puncture, rabbit ear scratch, and rabbit kidney scratch experiments. In these experiments, HR50(u3) samples were used as the experimental group, while Gelatin (at the same volume as HR50(u3))

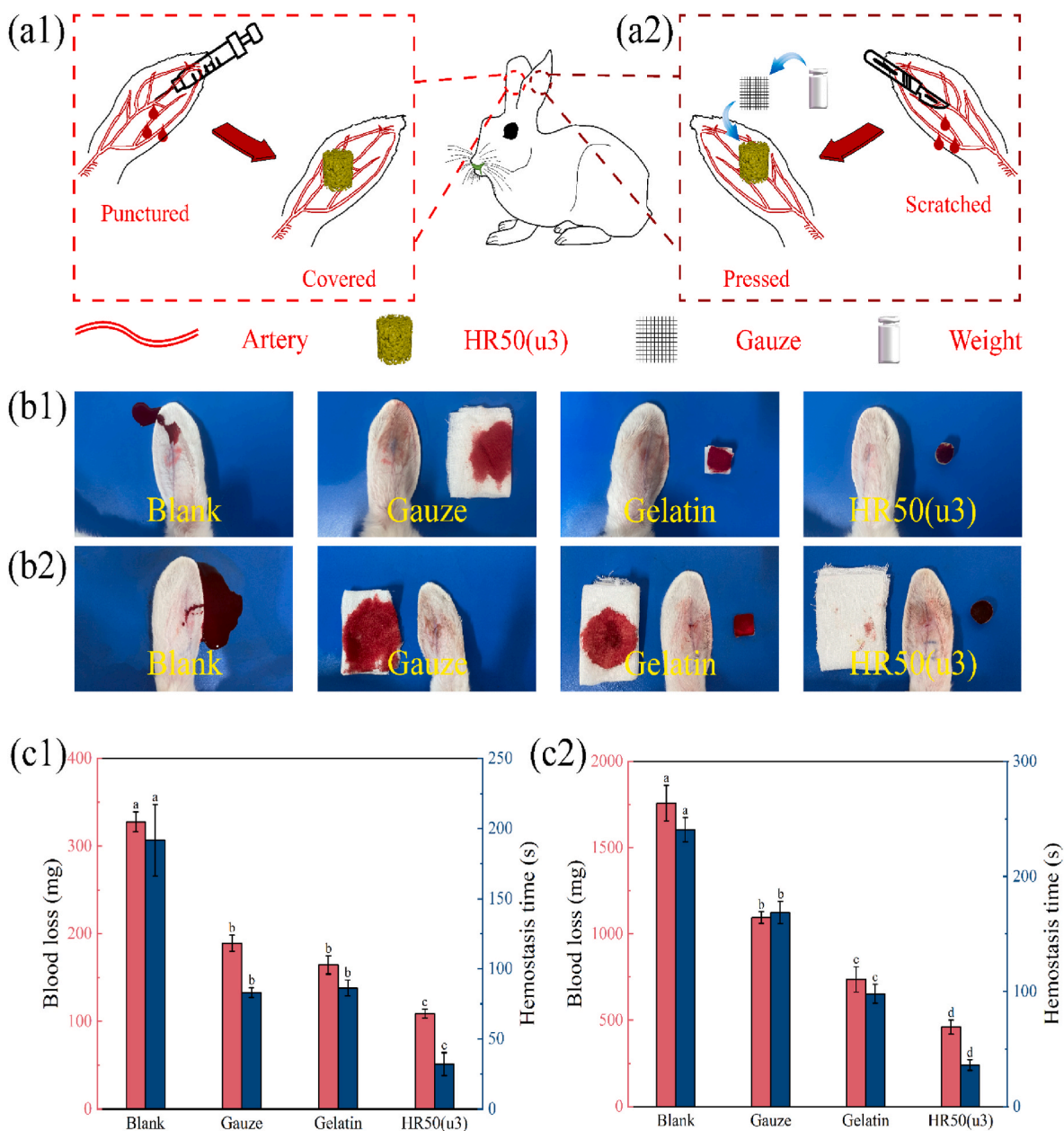


Fig. 8. Schematic diagram illustrating the (a1) rabbit ear puncture hemostatic model, (a2) rabbit ear scratch hemostatic model. Hemostatic effects of control and sample groups observed during (b1) rabbit ear puncture experiment, (b2) rabbit ear scratch experiment. Blood loss and hemostasis time of control and sample groups in (c1) rabbit ear puncture experiment, (c2) rabbit ear scratch experiment. Different letters in the bar chart indicate significant differences ($p < 0.05$) between samples.

and Gauze served as control groups. The blank group consisted of animals without any treatment. Schematic diagrams of the rabbit ear puncture and rabbit ear scratch experiments are presented in Fig. 8(a1, a2).

Fig. 8(b1, b2) shows the blood loss images of the blank group, as well as the control and experimental groups after hemostasis. It is evident that in cases of minimal bleeding, both Gauze and Gelatin are able to completely absorb the blood. However, the results of blood loss and bleeding time experiments (Fig. 8(c1)) demonstrate that the sample group (HR50(u3)) significantly reduce blood loss and bleeding time, indicating its excellent hemostatic performance. To further validate the hemostatic capability of the samples, gauze was placed over HR50(u3) and Gelatin during the rabbit ear scratching experiment (Fig. 8(a2)) to collect the blood that did not enter the samples. Fig. 8(c2) illustrates the experimental results after hemostasis. The gauze covering HR50(u3)

exhibits minimal blood exudation, indicating its efficient fluid absorption and coagulation ability. In contrast, a substantial amount of blood flowed through Gelatin and was subsequently absorbed by the covering gauze. This result suggests that Gelatin could only absorb blood through physical action when faced with a significant amount of bleeding, thereby failing to achieve rapid hemostasis.

Moreover, to comprehensively evaluate the hemostatic ability of the samples, an emergency haemorrhage-hemostasis experiment was conducted on a non-compressible rabbit kidney. The schematic diagram of the experiment is presented in Fig. 9(a). Fig. 9(b) displays images of the different treatments applied to the wounds after being scratched. In the blank group (without any hemostatic treatment), a greater amount of blood flowed out within a short period of time. In the Gelatin and Gauze hemostasis group, more blood was still absorbed on the filter paper (15 cm in diameter). Conversely, in the HR50(u3) treatment group, most

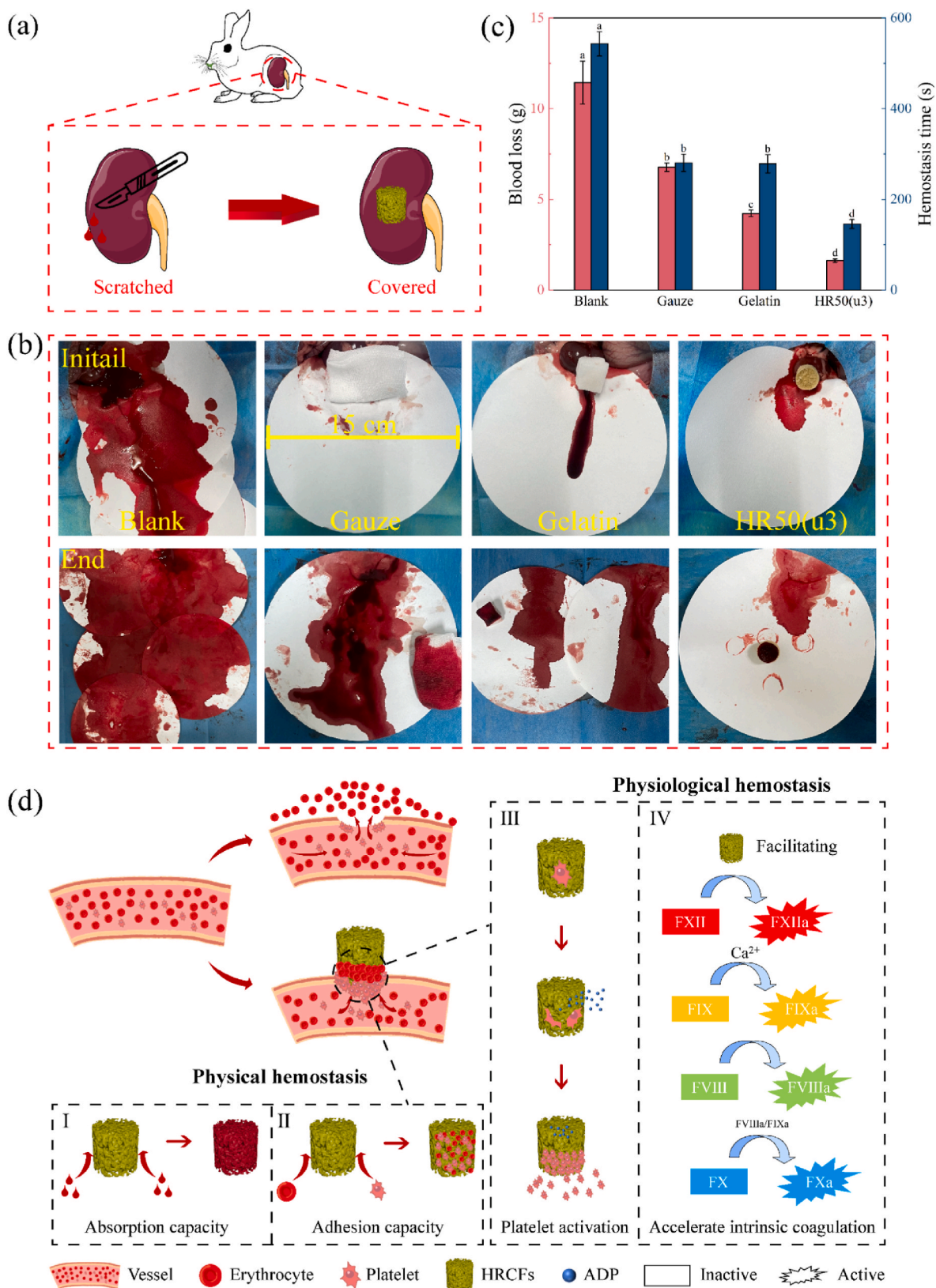


Fig. 9. (a) Schematic diagram illustrating the rabbit kidney scratch hemostatic model. (b) Hemostatic effects of HR50(u3) observed during rabbit kidney scratch experiment. (c) Blood loss and hemostasis time of control and sample groups in rabbit kidney scratch experiment; different letters in the bar chart indicate significant differences ($p < 0.05$) between samples. (d) Hemostatic mechanisms of HRCFs: (I) the porous structure possesses the ability to rapidly absorb blood, (II) the porous structure creates an optimal environment for the adhesion and accumulation of blood cells, (III) collagen stimulates platelets to release ADP and promotes platelets activation and aggregation, (IV) collagen plays a role in aiding and accelerating the endogenous coagulation process.

blood can be absorbed by sample. The results of blood loss and hemostasis time (Fig. 9(c)) demonstrate that the sample-treated group exhibited lower blood loss compared to the blank group, and the hemostasis time was significantly shorter. These results indicate that HR50 (u3) possesses excellent hemostatic ability, which could be attributed to the rapid liquid absorption capability (capillary effect) of HR50(u3) and the coagulation effect of collagen fibers.

Hemostasis is typically achieved through two processes: physical hemostasis and physiological hemostasis. Physical hemostasis primarily relies on the porous structure of the material, while physiological hemostasis involves the interaction between the hemostatic material and platelets, as well as its direct or indirect involvement in the coagulation process. Based on the results of *in vitro* coagulation experiments and animal experiments, the hemostatic mechanisms for HRCFs were speculated (Fig. 9(d)). HRCFs possess a porous structure that facilitates rapid blood absorption through capillary effect, leading to the adhesion and aggregation of blood cells on the inner walls of the pores. Additionally, collagen can facilitate the endogenous coagulation process, thereby contributing to rapid hemostasis [45].

4. Conclusions

In this study, a dual green strategy was developed from raw material to preparation process. The microfibers were obtained by breaking the connection between collagen fiber aggregates in inner tissues of HR and then transformed into highly absorbent sponges with a capillary effect through one-step freeze-drying. The process utilizes marine waste as raw materials, allows for reagent recovery and recycling, and ensures complete natural degradation, aligning with sustainable development principles. The collagen fiber sponges exhibit strong clotting ability, blood cell aggregation, platelet activation and ideal biocompatibility. Compared to commercial hemostatic materials, HRCFs significantly reduce blood loss and hemostasis time. This dual green strategy offers valuable insights for the development of environmentally friendly hemostatic materials.

Funding statement

This work was financially supported by the National Natural Science Foundation of China (Grant No. 22078060 and 22178056), Fujian Provincial Science and Technology Major Project (Grant No.2023YZ038001), the Natural Science Foundation of Fujian Province (Grant No. 2021J01665), High-level introduction project of Fujian Province (Grant No. XRCZX2018008).

CRediT authorship contribution statement

Cuicui Ding: Conceptualization, Formal analysis, Funding acquisition, Supervision, Writing – review & editing. **Kuan Cheng:** Data curation, Investigation, Software, Writing – original draft. **Yue Wang:** Investigation, Software. **Yifan Yi:** Investigation, Software. **Xiaohong Chen:** Investigation, Methodology. **Jingyi Li:** Investigation, Writing – review & editing. **Kaiwen Liang:** Investigation, Software. **Min Zhang:** Conceptualization, Funding acquisition, Project administration, Resources, Supervision, Writing – review & editing.

Declaration of competing interest

None.

Data availability

Data will be made available on request.

Appendix A. Supplementary data

Supplementary data to this article can be found online at <https://doi.org/10.1016/j.mtbio.2024.100946>.

References

- [1] X. Peng, X. Xu, Y. Deng, X. Xie, L. Xu, X. Xu, W. Yuan, B. Yang, X. Yang, X. Xia, L. Duan, L. Bian, Ultrafast self-gelling and wet adhesive powder for acute hemostasis and wound healing, *Adv. Funct. Mater.* 31 (33) (2021) 2102583.
- [2] H. He, W. Zhou, J. Gao, F. Wang, S. Wang, Y. Fang, Y. Gao, W. Chen, W. Zhang, Y. Weng, Z. Wang, H. Liu, Efficient, biosafe and tissue adhesive hemostatic cotton gauze with controlled balance of hydrophilicity and hydrophobicity, *Nat. Commun.* 13 (1) (2022) 552.
- [3] Y. Huang, X. Zhao, Z. Zhang, Y. Liang, Z. Yin, B. Chen, L. Bai, Y. Han, B. Guo, Degradable gelatin-based IPN cryogel hemostat for rapidly stopping deep noncompressible hemorrhage and simultaneously improving wound healing, *Chem. Mater.* 32 (15) (2020) 6595–6610.
- [4] Y. Wan, J. Han, F. Cheng, X. Wang, H. Wang, Q. Song, W. He, Green preparation of hierarchically structured hemostatic epoxy-amine sponges, *Chem. Eng. J.* 397 (2020) 125445.
- [5] X. Lu, Z. Liu, Q. Jia, Q. Wang, Q. Zhang, X. Li, J. Yu, B. Ding, Flexible bioactive glass nanofiber-based self-expanding cryogels with superelasticity and bioadhesion enabling hemostasis and wound healing, *ACS Nano* 17 (12) (2023) 11507–11520.
- [6] Q. Yang, J. Zhao, A. Muhammad, L. Tian, Y. Liu, L. Chen, P. Yang, Biopolymer coating for particle surface engineering and their biomedical applications, *Materials Today Bio* 16 (2022) 100407.
- [7] M. Zhang, Q. Yang, T. Hu, L. Tang, Y. Ni, L. Chen, H. Wu, L. Huang, C. Ding, Adhesive, antibacterial, conductive, anti-UV, self-healing, and tough collagen-based hydrogels from a pyrogallol-Ag self-catalysis system, *ACS Appl. Mater. Interfaces* 14 (7) (2022) 8728–8742.
- [8] L. Qi, L. Mu, X. Guo, A. Liu, C. Chen, Q. Ye, Z. Zhong, X. Shi, Fast expandable chitosan-fibers cryogel from ambient drying for noncompressible bleeding control and *in situ* tissue regeneration, *Adv. Funct. Mater.* 33 (16) (2023) 2212231.
- [9] S. Cao, Q. Li, S. Zhang, Z. Liu, X. Lv, J. Chen, Preparation of biodegradable carboxymethyl cellulose/dopamine/Ag NPs cryogel for rapid hemostasis and bacteria-infected wound repair, *Int. J. Biol. Macromol.* 222 (Pt A) (2022) 272–284.
- [10] L.P. Datta, S. Manchineella, T. Govindaraju, Biomolecules-derived biomaterials, *Biomaterials* 230 (2020) 119633.
- [11] S. Jiao, X. Zhang, H. Cai, S. Wu, X. Ou, G. Han, J. Zhao, Y. Li, W. Guo, T. Liu, W. Qu, Recent advances in biomimetic hemostatic materials, *Materials Today Bio* 19 (2023) 100592.
- [12] C.-Y. Zou, Q.-J. Li, J.-J. Hu, Y.-T. Song, Q.-Y. Zhang, R. Nie, J. Li-Ling, H.-Q. Xie, Design of biopolymer-based hemostatic material: starting from molecular structures and forms, *Materials Today Bio* 17 (2022) 100468.
- [13] J.-t. Gu, K. Jiao, J. Li, J.-f. Yan, K.-y. Wang, F. Wang, Y. Liu, F.R. Tay, J.-h. Chen, L.-n. Niu, Polyphosphate-crosslinked collagen scaffolds for hemostasis and alveolar bone regeneration after tooth extraction, *Bioact. Mater.* 15 (2022) 68–81.
- [14] T. Yan, F. Cheng, X. Wei, Y. Huang, J. He, Biodegradable collagen sponge reinforced with chitosan/calcium pyrophosphate nanoflowers for rapid hemostasis, *Carbohydr. Polym.* 170 (2017) 271–280.
- [15] S. Lv, M. Cai, F. Leng, X. Jiang, Biodegradable carboxymethyl chitin-based hemostatic sponges with high strength and shape memory for non-compressible hemorrhage, *Carbohydr. Polym.* 288 (2022) 119369.
- [16] C. Ding, M. Tian, Y. Wang, K. Cheng, Y. Yi, M. Zhang, Governing the aggregation of type I collagen mediated through β -cyclodextrin, *Int. J. Biol. Macromol.* 240 (2023) 124469.
- [17] M. Zhang, F. Deng, L. Tang, H. Wu, Y. Ni, L. Chen, L. Huang, X. Hu, S. Lin, C. Ding, Super-ductile, injectable, fast self-healing collagen-based hydrogels with multi-responsive and accelerated wound-repair properties, *Chem. Eng. J.* 405 (2021) 126756.
- [18] L. Zhu, J. Li, Y. Wang, X. Sun, B. Li, S. Pongchawanwong, H. Hou, Structural feature and self-assembly properties of type II collagens from the cartilages of skate and sturgeon, *Food Chem.* 331 (2020) 127340.
- [19] M. Govindharaj, U.K. Roopavath, S.N. Rath, Valorization of discarded Marine Eel fish skin for collagen extraction as a 3D printable blue biomaterial for tissue engineering, *J. Clean. Prod.* 230 (2019) 412–419.
- [20] G. Selvakumar, I. Kuttalam, S. Mukundan, S. Lonchin, Valorization of toxic discarded fish skin for biomedical application, *J. Clean. Prod.* 323 (2021) 129147.
- [21] D.N. Carvalho, D.S. Williams, C.G. Sotelo, R.I. Pérez-Martín, A. Mearns-Spragg, R. L. Reis, T.H. Silva, Marine origin biomaterials using a compressive and absorption methodology as cell-laden hydrogel envisaging cartilage tissue engineering, *Biomater. Adv.* 137 (2022) 212843.
- [22] S. Mizuta, S. Isobe, R. Yoshinaka, Existence of two molecular species of collagen in the muscle layer of the ascidian (*Halocynthia roretzi*), *Food Chem.* 79 (1) (2002) 9–13.
- [23] G. Lambert, Invasive sea squirts: a growing global problem, *J. Exp. Mar. Biol. Ecol.* 342 (1) (2007) 3–4.
- [24] C.K. Kang, E.J. Choy, Y.B. Hur, J.I. Myeong, Isotopic evidence of particle size-dependent food partitioning in cocultured sea squirt *Halocynthia roretzi* and Pacific oyster *Crassostrea gigas*, *Aquat. Biol.* 6 (2009) 289–302.
- [25] L. Manni, F. Caicci, C. Anselmi, V. Vanni, S. Mercurio, R. Pennati, Morphological study and 3D reconstruction of the larva of the ascidian *Halocynthia roretzi*, *J. Mar. Sci. Eng.* 10 (1) (2022) 11.

- [26] Y. Yang, Y. Zhu, H. Liu, J. Wei, H. Yu, B. Dong, Cultivation of gut microorganisms of the marine ascidian *Halocynthia roretzi* reveals their potential roles in the environmental adaptation of their host, *Marine Life Science & Technology* 4 (2) (2022) 201–207.
- [27] G. Song, J. Delroisse, D. Schoenaers, H. Kim, T.C. Nguyen, N. Horbelt, P. Leclère, D. S. Hwang, M.J. Harrington, P. Flammang, Structure and composition of the tunic in the sea pineapple *Halocynthia roretzi*: a complex cellulosic composite biomaterial, *Acta Biomater.* 111 (2020) 290–301.
- [28] Y. He, Q. Li, P. Chen, Q. Duan, J. Zhan, X. Cai, L. Wang, H. Hou, X. Qiu, A smart adhesive Janus hydrogel for non-invasive cardiac repair and tissue adhesion prevention, *Nat. Commun.* 13 (1) (2022) 7666.
- [29] Y. He, H. Hou, S. Wang, R. Lin, L. Wang, L. Yu, X. Qiu, From waste of marine culture to natural patch in cardiac tissue engineering, *Bioact. Mater.* 6 (7) (2021) 2000–2010.
- [30] J. Li, S. Han, Y. Zhu, B. Dong, A. Halorotetin, A novel terpenoid compound isolated from ascidian *Halocynthia roretzi* exhibits the inhibition activity on tumor cell proliferation, *Mar. Drugs* 21 (1) (2023) 51.
- [31] Y. Zhu, H. Gao, S. Han, J. Li, Q. Wen, B. Dong, Antidiabetic activity and metabolite profiles of ascidian *Halocynthia roretzi*, *J. Funct. Foods* 93 (2022) 105095.
- [32] S. Pezeshk, M. Rezaei, M. Abdollahi, Impact of ultrasound on extractability of native collagen from tuna by-product and its ultrastructure and physicochemical attributes, *Ultrason. Sonochem.* 89 (2022) 106129.
- [33] L. Wang, Q. Liang, T. Chen, Z. Wang, J. Xu, H. Ma, Characterization of collagen from the skin of Amur sturgeon (*Acipenser schrenckii*), *Food Hydrocolloids* 38 (2014) 104–109.
- [34] J. Cai, L. Zhang, J. Zhou, H. Li, H. Chen, H. Jin, Novel fibers prepared from cellulose in NaOH/urea aqueous solution, *Macromol. Rapid Commun.* 25 (17) (2004) 1558–1562.
- [35] Q. Yang, C. Guo, F. Deng, C. Ding, J. Yang, H. Wu, Y. Ni, L. Huang, L. Chen, M. Zhang, Fabrication of highly concentrated collagens using cooled urea/HAc as novel binary solvent, *J. Mol. Liq.* 291 (2019) 111304.
- [36] Y. Pei, K.E. Jordan, N. Xiang, R.N. Parker, X. Mu, L. Zhang, Z. Feng, Y. Chen, C. Li, C. Guo, K. Tang, D.L. Kaplan, Liquid-exfoliated mesostructured collagen from the bovine achilles tendon as building blocks of collagen membranes, *ACS Appl. Mater. Interfaces* 13 (2) (2021) 3186–3198.
- [37] S. Yang, S.A. Madbouly, J.A. Schrader, G. Srinivasan, D. Grewell, K.G. McCabe, M. R. Kessler, W.R. Graves, Characterization and biodegradation behavior of bio-based poly(lactic acid) and soy protein blends for sustainable horticultural applications, *Green Chem.* 17 (1) (2015) 380–393.
- [38] Z. Xu, L. Zou, F. Xie, X. Zhang, X. Ou, G. Gao, Biocompatible carboxymethyl chitosan/GO-based sponge to improve the efficiency of hemostasis and wound healing, *ACS Appl. Mater. Interfaces* 14 (39) (2022) 44799–44808.
- [39] W. Zheng, Z. Zhang, Y. Li, L. Wang, F. Fu, H. Diao, X. Liu, A novel pullulan oxidation approach to preparing a shape memory sponge with rapid reaction capability for massive hemorrhage, *Chem. Eng. J.* 447 (2022) 137482.
- [40] H. Cheng, X. Pan, Z. Shi, X. Huang, Q. Zhong, H. Liu, Y. Chen, Q. Lian, J. Wang, Z. Shi, Chitin/corn stalk pith sponge stimulated hemostasis with erythrocyte absorption, platelet activation, and Ca²⁺-binding capabilities, *Carbohydr. Polym.* 284 (2022) 118953.
- [41] L. Cui, J. Li, S. Guan, K. Zhang, K. Zhang, J. Li, Injectable multifunctional CMC/HADA hydrogel for repairing skin injury, *Materials Today Bio* 14 (2022) 100257.
- [42] Y. Yang, Y. Zhang, Y. Min, J. Chen, Preparation of methacrylated hyaluronate/methacrylated collagen sponges with rapid shape recovery and orderly channel for fast blood absorption as hemostatic dressing, *Int. J. Biol. Macromol.* 222 (2022) 30–40.
- [44] L. Wang, Y. Zhong, C. Qian, D. Yang, J. Nie, G. Ma, A natural polymer-based porous sponge with capillary-mimicking microchannels for rapid hemostasis, *Acta Biomater.* 114 (2020) 193–205.
- [45] Y. Cheng, S. Lu, Z. Hu, B. Zhang, S. Li, P. Hong, Marine collagen peptide grafted carboxymethyl chitosan: optimization preparation and coagulation evaluation, *Int. J. Biol. Macromol.* 164 (2020) 3953–3964.
- [46] C. Liu, X. Liu, C. Liu, N. Wang, H. Chen, W. Yao, G. Sun, Q. Song, W. Qiao, A highly efficient, in situ wet-adhesive dextran derivative sponge for rapid hemostasis, *Biomaterials* 205 (2019) 23–37.
- [47] Y. Huang, X. Zhao, C. Wang, J. Chen, Y. Liang, Z. Li, Y. Han, B. Guo, High-strength anti-bacterial composite cryogel for lethal noncompressible hemorrhage hemostasis: synergistic physical hemostasis and chemical hemostasis, *Chem. Eng. J.* 427 (2022) 131977.
- [48] N.K. Vate, I. Undeland, M. Abdollahi, Resource efficient collagen extraction from common starfish with the aid of high shear mechanical homogenization and ultrasound, *Food Chem.* 393 (2022) 133426.
- [49] Y. Fan, Q. Lu, W. Liang, Y. Wang, Y. Zhou, M. Lang, Preparation and characterization of antibacterial polyvinyl alcohol/chitosan sponge and potential applied for wound dressing, *Eur. Polym. J.* 157 (2021).
- [50] Y. Cui, Y. Wang, Z. Shao, A. Mao, W. Gao, H. Bai, Smart sponge for fast liquid absorption and thermal responsive self-squeezing, *Adv. Mater.* 32 (14) (2020) 1908249.
- [51] M. Zhou, J. Liao, G. Li, Z. Yu, D. Xie, H. Zhou, F. Wang, Y. Ren, R. Xu, Y. Dai, J. Wang, J. Huang, R. Zhang, Expandable carboxymethyl chitosan/cellulose nanofiber composite sponge for traumatic hemostasis, *Carbohydr. Polym.* 294 (2022) 119805.
- [52] X. Tong, Z. Shi, L. Xu, J. Lin, D. Zhang, K. Wang, Y. Li, C. Wen, Degradation behavior, cytotoxicity, hemolysis, and antibacterial properties of electro-deposited Zn–Cu metal foams as potential biodegradable bone implants, *Acta Biomater.* 102 (2020) 481–492.